Supersonic Separated Flow past a Cylindrical Obstacle on a Flat Plate

Oktay Özcan* and Maurice Holt†
University of California, Berkeley, California

An experimental investigation of three-dimensional boundary-layer separation on a flat plate ahead of a circular cylinder at Mach 2.36 was made. Emphasis was given given to the laminar flow regime and to the flow region upstream of the cylinder. The heights and diameters of the cylinders used in the study were larger than the undisturbed boundary-layer thickness at the cylinder location. Data were obtained by oil flow visualization, schlieren observations, static pressure measurements, and laser anemometry. Oil flow visualization revealed three separation lines on the flat plate ahead of the cylinder. A postulated flowfield structure, which was suggested by this skin-friction pattern, could not be confirmed by the velocity measurements. Velocity measurements indicated an unsteady flow structure.

Nomenclature

D = cylinder diameter
H = cylinder height
L = distance along symmetry axis between flat plate leading edge and cylinder axis
ℓ = distance along symmetric axis between flat plate leading edge and primary separation line (L-S-$D/2$)
M = Mach number
p = static pressure
Re = Reynolds number
S = distance along symmetry axis between cylinder leading edge and primary separation line
U, W = velocities in X and Z directions
X, Y, Z = streamwise, spanwise, and vertical directions (Fig. 1)
δ = boundary-layer thickness

Subscripts

0 = conditions upstream of interaction
1 = plate 1
2 = plate 2
e = edge of boundary layer
p = plateau

I. Introduction

IN high-speed flow past a blunt protuberance on a flat plate, a detached bow shock is formed ahead of the protuberance. The adverse pressure gradient, caused by the detached shock wave, propagates upstream through the subsonic portion of the boundary layer and leads to the separation of the boundary layer on the flat plate. A number of vortices are formed in the separated flow region ahead of the protuberance.[1] These vortices scavenge part of the freestream flow toward the surface and spiral downstream. The major effects of the shock-wave/boundary-layer interaction are increased pressure loads and heat transfer levels on and in the vicinity of the protuberance. Korkegi[2] reports that such interactions have caused structural damage on hypersonic aircraft wing-body junctions.

Received Feb. 11, 1983; revision received June 24, 1983.

*National Research Council Associate, NASA Ames Research Center, Moffett Field, Calif.
†Professor, Department of Mechanical Engineering.

Sedney[3] classifies protuberances as small and large depending on their height H relative to the boundary-layer thickness δ. A protuberance is considered small if H/δ is of order one or less and if its effect on the freestream flow is small. A survey of small protuberance/boundary-layer interactions is given by Ref. 3. For turbulent high-speed flow, there is a large body of references which reveal the flow pattern in terms of surface flowfield, surface pressures and heat rates, and protuberance pressures and heat rates. Korkegi[2] gives a survey of experimental data for large protuberances in high-speed flows. In turbulent flow past semi-infinite cylinders (or blunt fins), separation occurs typically two to three cylinder diameters upstream of the cylinder leading edge. The extent of separation depends weakly on Reynolds number,[4] incoming boundary-layer thickness,[5] and Mach number[6] and is primarily dependent on protuberance geometry. Unsteady aspects of the turbulent flow interaction are discussed in Refs. 4-6.

There are limited experimental data for laminar high-speed flows. Avduevskii and Medvedev[7] report separation distance correlations for flow past cylinders and parallelepipeds at $M=2$-6. Young et al.[8] give surface flow and static pressure at $M=3$ and 5. Reference 8 also reports total pressure data and notes that the presence of a probe in a separated flow region alters the flowfield significantly. Hung and Clauss[9] report surface temperature measurements for laminar flow past cylinders at $M=5.3$.

The purpose of the present study was to obtain a detailed data set, including velocity measurements, for laminar flow past a circular cylinder. The heights of the cylinders used in the study were 7 to 30 times larger than the undisturbed boundary-layer thickness at the cylinder location. Therefore, all cylinders of the study were long protuberances by Sedney's definition.[3] (Note that this definition of a long protuberance does not stipulate an "asymptotic result" which occurs when the extent of separation does not increase with an increase in protuberance height.) Oil flow visualization was employed to determine the global structure of the flow and to obtain separation distance measurements. Static pressure measurements on the symmetry axis of the interaction were made for various cylinders. Detailed velocity and static pressure data were obtained for a particular cylinder. A single-component, differential (dual) beam laser-velocimeter was used to measure streamwise and vertical velocities. A detailed description and results of the study, including surface flow data for transitional and turbulent flow regimes, were reported in Ref. 10.

II. Experimental Apparatus and Conditions

A. Wind Tunnel and Models

The experiments were carried out in the Hesse Hall 15 × 15-cm supersonic wind tunnel at the University of California, Berkeley. This facility is a closed-cycle, variable density wind tunnel. The diameter D, height-to-diameter ratio H/D, and symbol of the cylinders used in the study are given in Table 1. The cylinders were interchangeably mounted on a flat plate which was secured to the tunnel floor by two posts. The flat plate, with a leading-edge thickness less than 0.07 mm, spanned the test section and was sealed at the tunnel windows by rubber. Two plates, which differed only in L (the distance along the symmetry axis between the plate leading edge and the cylinder axis), were used. The overall dimensions of plate 1 ($L_1 = 150.8$ mm) and plate 2 ($L_2 = 76.2$ mm) are given in Fig. 1, which also shows the coordinate system chosen for data presentation.

B. Test Conditions

The wind tunnel was operated nominally at Mach 2.36. Stagnation temperature was held constant at 21°C. Unit Reynolds number was varied between 2.5×10^4 to 1.6×10^5 (1/cm) by changing tunnel stagnation pressure. Laminar flow test conditions were obtained at stagnation pressures 2.4×10^4 and 3.3×10^4 (N/m^2) which led to unit Reynolds numbers 2.5×10^4 and 3.5×10^4 (1/cm), respectively. The laminar flow regime was identified on the basis of Schlieren observations, separation distance correlations, and pressure measurements. The velocity measurements confirmed that the boundary layer was laminar over a large portion of the separated flow region. However, the inability of the laser-velocimeter to distinguish between unsteadiness and turbulence precluded any conclusions about the state of the boundary layer close to the cylinder.

C. Measurements and Associated Accuracies

Oil flow visualization data were obtained by an oil-film method which produced a clearer skin-friction pattern than the oil-streak method. Formation time of the oil flow pattern was typically 10 min. Separation distances were measured from the oil flow photographs which were taken during the tunnel run. The precision of the measurements was better than ±1.5 mm for the measurement of all separation distances. Since it was extremely difficult to observe the reattachment lines, the reattachment distances were not measured. Laminar oil flow visualization data were obtained for cylinders mounted on plate 1 at $Re_{L_1} = 3.8 \times 10^5$ and on plate 2 at $Re_{L_2} = 1.9 \times 10^5$ and 2.7×10^5.

Static pressures were measured by a differential pressure sensor whose accuracy was better than ±0.3% of the undisturbed pressure upstream of the interaction. Pressure data were obtained for various cylinders mounted on plate 1 at $Re_{L_1} = 3.8 \times 10^5$ along four streamwise lines ($Y = 0$, 12.7, 25.4, and 38.1 mm) and for cylinder 3 along four spanwise lines ($-X = 8.7$, 39.7, 74.6, and 100 mm). The spanwise symmetry of the pressure distribution was checked and confirmed. Measurements in the absence of a cylinder showed that the flow over the flat plate was free from any wind-tunnel disturbance.

The streamwise and vertical velocities (U and W) were measured by a single-component, forward scatter, differential (dual) beam laser-velocimeter. A Laskin type aerosol generator was used to seed the flow. A 30 MHz Bragg shift in the positive X and Z directions was employed to resolve the direction of velocities. The width and the length of the scattering volume were 0.18 and 2 mm, respectively. Mean velocity errors due to velocity lag and noise in signal were shown to be negligible. Errors due to high-velocity biasing and velocity gradients across scattering volume were less than 2% and 1%, respectively. Velocity measurements were made for cylinder 3 mounted on plate 1 at $Re_{L_1} = 3.8 \times 10^5$. The measured value of the undisturbed boundary-layer thickness was 1.86 mm. The freestream velocity did not change by more than 1.3% between the flat plate leading edge and the cylinder location. The freestream turbulence was less than 1%.

III. Results and Discussion

A. Schlieren Observations

Figure 2 shows a schlieren photograph of the flowfield for cylinder 3 mounted on plate 1 at $Re_{L_1} = 3.8 \times 10^5$. The flow direction is from right to left. The bright edge of the laminar boundary layer can be seen to persist up to three cylinder diameters downstream of the cylinder. The λ leg of the detached bow shock is rather weak and cannot be observed in Fig. 2.

B. Oil Flow Visualization

Figure 3 gives the oil flow pattern for cylinder 7 mounted on plate 1 at $Re_{L_1} = 3.8 \times 10^5$. The flow direction is from right to left. Three separation lines on the flat plate ahead of the cylinder can be observed. The separation lines are labeled as,

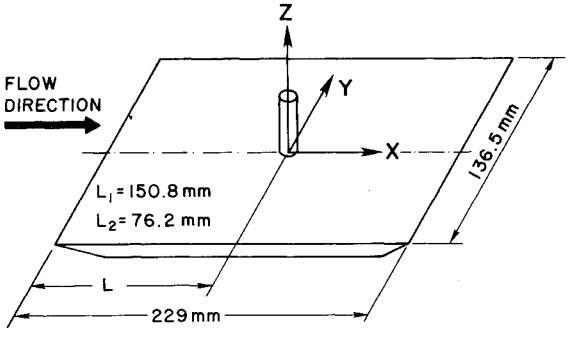

Fig. 1 Definition of coordinate system and overall dimensions of plates 1 and 2.

Table 1 Separation distances for cylinders mounted on plate 1 at $Re_{L_1} = 3.8 \times 10^5$

Symbol	D, mm	H/D	S/D	$Re_l \times 10^{-5}$
1	3.97	11	7.6	3.1
2	4.76	8	7.6	3.0
5	7.94	8	7.6	2.9
7	6.35	4	7.2	2.7
4	4.76	7	7.2	2.7
8	7.94	3.5	6.7	2.5
3	6.35	8	6.6	2.5
6	7.94	4.5	6.6	2.5
9	9.53	2.5	6.1	2.4
10	9.53	1.5	5.7	2.4
11	12.70	1	4.3	2.5

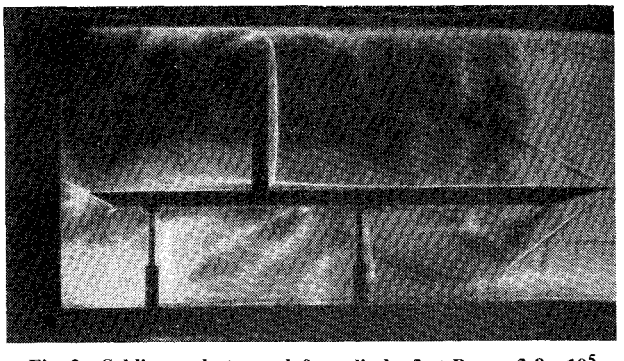

Fig. 2 Schlieren photograph for cylinder 3 at $Re_{L_1} = 3.8 \times 10^5$.

from right to left in Fig. 3, primary, tertiary, and secondary separation lines. The number of separation lines dropped from 3 to 2 and from 2 to 1 as Re_L was increased from 1.9×10^5 to 2.3×10^6. The variation of the surface flow structure with Reynolds number was reported in detail in Ref. 10. Sedney and Kitchens[1] observe three separation lines ahead of small cylinders in low Reynolds number turbulent flow at $M=2.5$ and 3.5. Young et al.[8] also report some evidence of a third separation line in laminar flow past fins at $M=3$ and 5.

Figure 4 gives a sketch of a postulated streamline pattern on the symmetry axis which is consistent with the presence of three separation lines ahead of the cylinder. For the sake of clarity, the vertical distance is stretched and the shock structure is omitted. The locations of the three separation lines, as determined from oil flow photographs, are also given for cylinder 3. Such a streamline pattern was originally postulated by Sedney and Kitchens.[1] It will be suggested in Sec. III.D. that the streamline pattern given by Fig. 4 is one of the possible streamline patterns that succeed each other in time.

The extent of separation is characterized by the separation distance S, which is measured from the primary separation line to the cylinder leading edge along the symmetry axis. For laminar flow past long protuberances, Refs. 7 and 8 report that the extent of separation correlates with Reynolds number based on ℓ, which is the distance between the flat plate leading edge and the primary separation line. Tables 1 and 2 give the separation distance S (nondimensionalized with cylinder diameter) and Re_ℓ values for cylinders mounted on plates 1 and 2, respectively. The precision of S/D measurement is ±0.2. Inspection of Tables 1 and 2 shows that the dimensionless parameters governing the interaction are cylinder height-to-diameter ratio (H/D) and Re_ℓ. S/D increases from 3.0 to 7.6 as Re_ℓ increases from 1×10^5 to 3.1×10^5 and H/D increases from 1 to 11. For height-to-diameter ratios larger than 3.5, S/D increases with increasing Re_ℓ and is independent of H/D. For $H/D<4$, S/D increases with increasing H/D and is a function of both Re_ℓ and H/D.

Based on surface temperature measurements, Hung and Clauss[8] find $S/D=9$-12 for laminar flow past semi-infinite cylinders at $M=5.5$. They assume that the separation location is where the surface temperature (or static pressure) begins to rise from the undisturbed value on the axis of symmetry. It will be shown in Sec. III.C. that such an assumption leads to overprediction of separation distances. Reference 3 recommends that a distinction should be made between the disturbed flow region and the separated flow region as determined from surface indicators. Young et al.[8] report that for laminar flow past fins at $M=3$, S/D increases from 4.1 to 6.8 as Re_ℓ increases from 0.5×10^5 to 8.6×10^5. They observe smaller S/D values at $M=5$. Reference 7 reports a maximum S/D value of 6 at $M=6$.

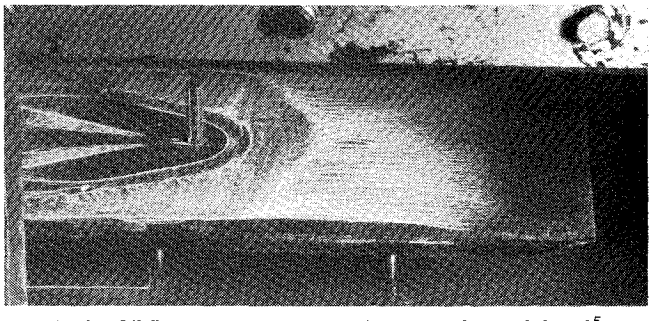

Fig. 3 Oil flow photograph for cylinder 7 at $Re_{L_l}=3.8\times10^5$.

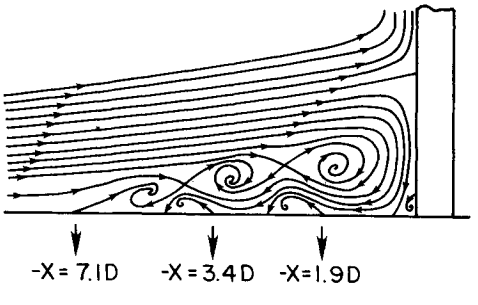

Fig. 4 Sketch of postulated streamline pattern on the symmetry axis.

C. Static Pressure Measurements

Figure 5 gives the streamwise pressure distribution on the axis of symmetry at $Re_{L_l}=3.8\times10^5$ for cylinders with height-to-diameter ratios ranging from 6 to 11. Cylinder leading edge is located at $-X/D=0.5$ and high pressures downstream of the bow shock are not shown. Pressure is nondimensionalized in terms of p_0 which is the undisturbed pressure upstream of the interaction. p_0 is nominally 1.8×10^3 N/m^2. The oil flow visualization results show that the extent of separation is independent of height-to-diameter ratio for $H/D>4$. Therefore, it is expected that the pressure distributions given in Fig. 5 are independent of H/D and depend only on Re_ℓ. Figure 5 reveals that the initial pressure rise occurs further upstream, in terms of cylinder diameter, with increasing Re_ℓ. Figure 6 shows the streamwise pressure distribution along the axis of symmetry for cylinders 3, 6, 9, 10, and 11 at $Re_{L_l}=3.8\times10^5$. The Re_ℓ value associated with all of the cylinders is approximately 2.5×10^6. Therefore, it should be expected that Fig. 6 indicates the dependence of the pressure distribution on cylinder height-to-diameter ratio. It is observed readily that the extent of interaction, in terms of cylinder diameter, decreases with decreasing H/D values.

Figures 5 and 6 show that the pressure rise on the axis of symmetry begins as much as 12-cylinder diameters upstream of the cylinder leading edge. However, Table 1 reveals that separation occurs further downstream in the increasing

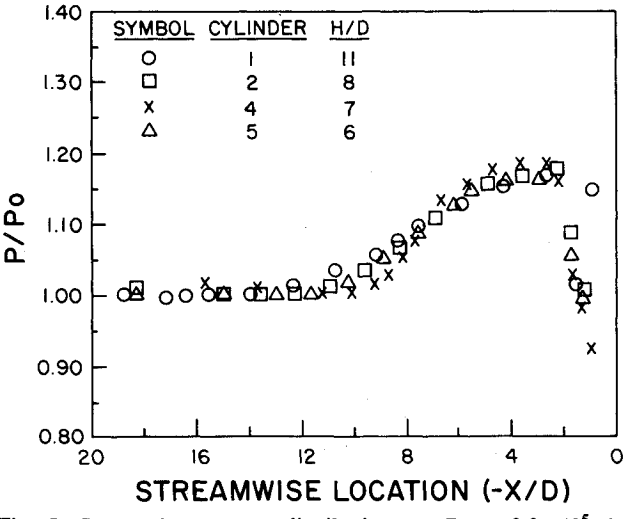

Fig. 5 Streamwise pressure distributions at $Re_{L_l}=3.8\times10^5$ for cylinders 1, 2, 4, and 5 along $Y/D=0$.

Table 2 Separation distances for cylinders mounted on plate 2 at $Re_{L_2}=1.9\times10^5$ and 2.7×10^5

	$Re_{L_2}=1.9\times10^5$		$Re_{L_2}=2.7\times10^5$	
Symbol	S/D	$Re_\ell\times10^{-5}$	S/D	$Re_\ell\times10^{-5}$
2	4.7	1.4	4.9	1.9
7	4.4	1.2	4.8	1.6
3	4.3	1.0	4.6	1.4
9	3.9	1.0	4.1	1.3
11	3.0	1.0	3.1	1.3

pressure region between the initial pressure rise and pressure plateau (p_p). Downstream of the plateau region, the pressure drops significantly, reaches a minimum valley pressure and increases through the detached bow shock. The secondary separation occurs in the increasing pressure region for the reverse flow between the pressure valley and the pressure plateau. No significant pressure gradients can be observed around the tertiary separation line.

Hill[11] correlates extensive two-dimensional separated flow data and obtains the following expression for laminar pressure plateau level

$$p_p/p_0 = 1 + 1.218M_0^2[(M_0^2-1)Re_\ell]^{-1/4}$$

which is valid for any two-dimensional geometry causing separation. Hill's correlation is an expression for the "free-interaction hypothesis" which states that the pressure distribution in the vicinity of separation is independent of the geometry causing the separation and depends solely on the local flow conditions.[12] For the Re_ℓ range of the present study, Hill's correlation predicts $1.20 < p_p/p_0 < 1.21$ which is in close agreement with the measured plateau levels ($1.17 < p_p/p_0 < 1.21$). The validity of the free-interaction hypothesis on the symmetry axis of the interaction is also observed in Ref. 8. Hill's correlation predicts that p_p/p_0 (and, consequently, the strength of the λ leg of the bow shock) increases with decreasing Re_ℓ. The λ leg of the bow shock could, indeed, be observed in the schlieren pictures of the present study at $Re_\ell = 0.6 \times 10^5$.

The streamwise and spanwise pressure distributions for cylinder 3 at $Re_{L_l} = 3.8 \times 10^5$ are given in Figs. 7 and 8, respectively. The location of the initial pressure rise moves downstream with increasing Y/D. However, in terms of the distance between the detached bow shock and the initial pressure rise location, the upstream influence increases with increasing Y/D. The decreasing magnitude of the pressure dip away from the axis of symmetry shows that the vortices ahead of the cylinder become weaker with increasing Y/D. Large streamwise and spanwise pressure gradients are observed within approximately two-cylinder diameters vicinity of the cylinder axis.

D. Velocity Measurements

Figures 9-12 give the streamwise velocity profiles at various $-X/D$, Y/D locations for cylinder 3 at $Re_{L_l} = 3.8 \times 10^5$.

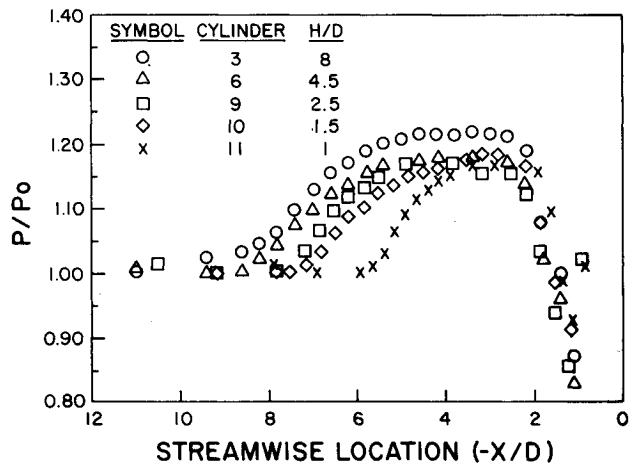

Fig. 6 Streamwise pressure distributions at $Re_{L_l} = 3.8 \times 10^5$ for cylinders 3, 6, 9, 10, and 11 along $Y/D = 0$.

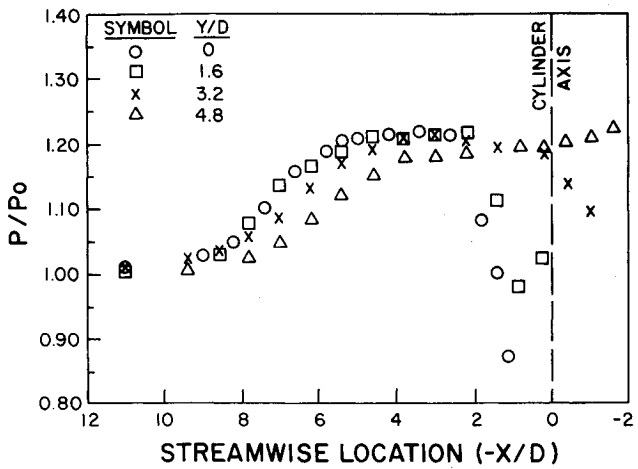

Fig. 7 Streamwise pressure distributions at $Re_{L_l} = 3.8 \times 10^5$ for cylinder 3 along $Y/D = 0$, 1.6, 3.2, and 4.8.

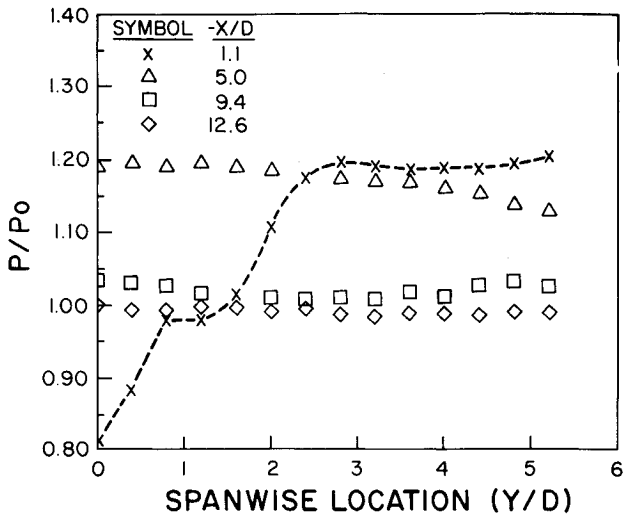

Fig. 8 Spanwise pressure distributions at $Re_{L_l} = 3.8 \times 10^5$ for cylinder 3 along $-X/D = 1.1$, 5.0, 9.4, and 12.6.

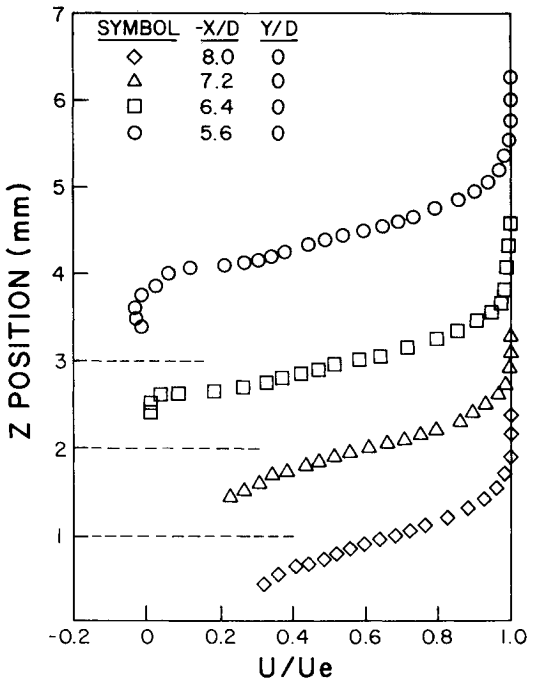

Fig. 9 Streamwise velocity profiles for cylinder 3 at $Y/D = 0$, $-X/D = 8$, 7.2, 6.4, and 5.6; and $Re_{L_l} = 3.8 \times 10^5$.

Velocities are nondimensionalized with respect to the freestream velocity U_e measured at the relevant $-X/D$, Y/D location. U_e is nominally 560 m/s. Dashed lines denote the U/U_e axis of the profiles whose origins are displaced from $Z=0$ to avoid overcrowding of the figures. The streamwise velocity profiles at $-X/D=8$, 7.2, 6.4, and 5.6 are given in Fig. 9. The profiles at $-X/D=8$ and 7.2 indicate preseparation behavior. The profile at $-X/D=6.4$ indicates that separation occurs in the close vicinity of $-X/D=6.4$. It is believed that separation occurred around $-X/D\sim 6.8$ where it was difficult to make repeatable velocity measurements due to the unsteadiness of the flow. Reverse flow cannot be detected at $-X/D=6.4$, probably due to the small scale of the reverse flow in the vicinity of the primary separation line. The velocity profile at $-X/D=5.6$ shows clearly the reverse flow region. Figure 10 presents the streamwise velocity profiles at $-X/D=4.8$, 4.0, and 3.2. The magnitude of the reverse velocities and the height of the reverse flow region increases with decreasing $-X/D$. The streamwise velocity profiles at $-X/D=2.4$ and 1.6 are given in Fig. 11. The magnitudes of the maximum reverse velocities are approximately equal at $-X/D=2.4$ and 1.6. However, the height of the reverse flow region decreases with decreasing $-X/D$. Figure 12 gives the velocity profiles at $-X/D=3.2$ for $Y/D=4.8$, 2.4, and 0. All profiles show postseparation behavior. The height of the reverse flow region and the magnitude of the reverse velocities decrease with increasing Y/D.

The streamwise velocity profiles at $-X/D=3.2$, 2.4, 1.6 and $Y/D=0$ exhibit significant kinks between the boundary-layer edge and the edge of the reverse flow region. A correlation between increasing unsteadiness and significant kinks was observed during the velocity measurements. Repeatability of the measurements for a certain number of velocity realizations was considered as a measure of the flow unsteadiness. For Z positions smaller than 0.6 mm, where the data acquisition time varied between 2 and 10 s, 512 or 1024 velocity realizations were taken for each data point. 2048 realizations were taken for $Z>0.6$ mm where the data acquisition time decreased monotonically from 2 to 0.5 s. All velocity measurements were then repeatable within ± 2 m/s. This repeatability bandwidth of the measurements was not affected by a decrease in the number of realizations from the earlier mentioned values for profiles at $-X/D\geq 4$ but increased for profiles at $-X/D<4$. Frequency range of the probability density functions (pdf's) also suggested an unsteady flow behavior. As an example, a velocity range between 80 and 440 m/s was typical for a data point with an average velocity of 292 m/s in regions of flow where the kinks were observed. The Gaussian shape of the pdf's suggested that the unsteady character of the flow could be cyclic (periodic).

Figure 13 gives the vertical velocity (W) profiles at $-X/D=4.8$, 4.0, 3.2, 2.4, and 1.6. Short lines on the right

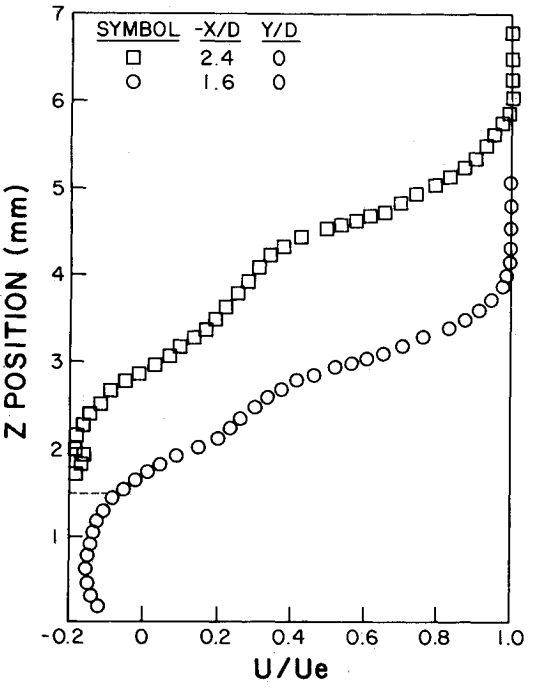

Fig. 11 Streamwise velocity profiles for cylinder 3 at $Y/D=0$, $-X/D=2.4$ and 1.6, and $Re_{L_I}=3.8\times 10^5$.

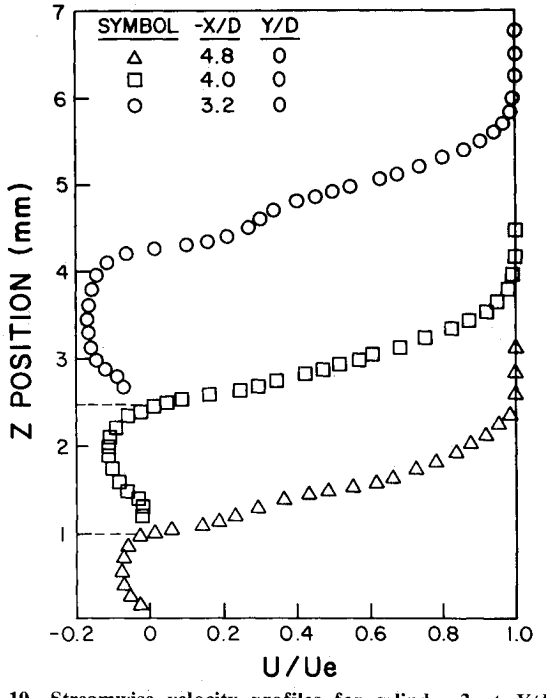

Fig. 10 Streamwise velocity profiles for cylinder 3 at $Y/D=0$, $-X/D=4.8$, 4.0, and 3.2 and $Re_{L_I}=3.8\times 10^5$.

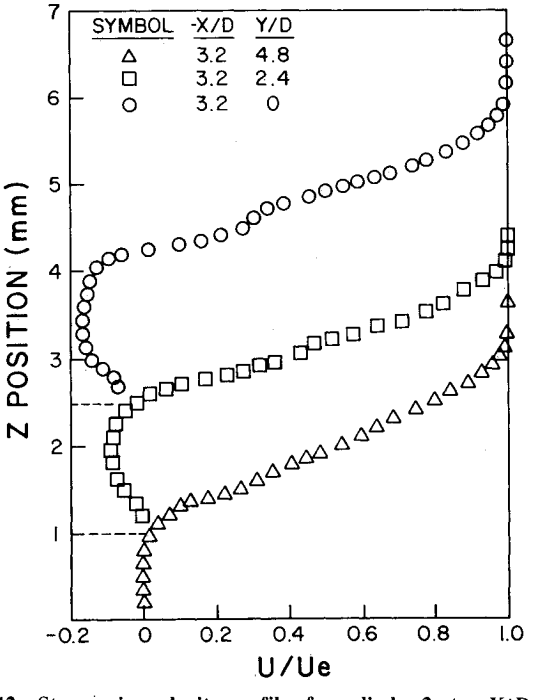

Fig. 12 Streamwise velocity profiles for cylinder 3 at $-X/D=3.2$, $Y/D=4.8$, 2.4, and 0, and $Re_{L_I}=3.8\times 10^5$.

frame of the figure denote the boundary-layer thickness as determined from the streamwise velocity measurements. For all profiles, magnitude of the vertical velocity is maximum around the boundary-layer edge and decreases with increasing Z in the freestream. Maximum reverse (toward the plate) velocities and height of the vertical flow region increases with decreasing $-X/D$. Figure 14 gives the vertical velocity and turbulence level profiles downstream of the detached bow shock at $-X/D=0.6$ and $Y/D=0$. The vertical velocity is nondimensionalized in terms of the freestream velocity upstream of the detached bow shock. Close to the cylinder root, the negative vertical velocity is as high as 20% of the freestream velocity and the turbulence level (W_{rms}/U_e) reaches 9%. Velocity measurements at $Re_{L_1}=2.3\times10^6$ showed that an order of magnitude increase in Reynolds number increased the maximum turbulence level from 9% merely to 10.5%. The weak dependence of the turbulence level on Reynolds number suggested that the unsteadiness of the flow was the main cause of the measured turbulence.

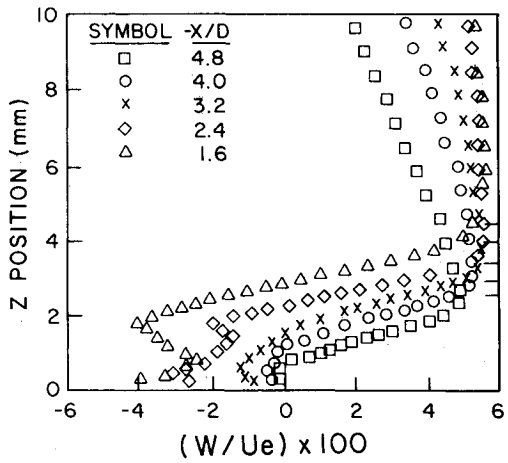

Fig. 13 Vertical velocity profiles for cylinder 3 at $Y/D=0$, $-X/D=4.8$, 4.0, 3.2, 2.4, and 1.6; and $Re_{L_1}=3.8\times10^5$.

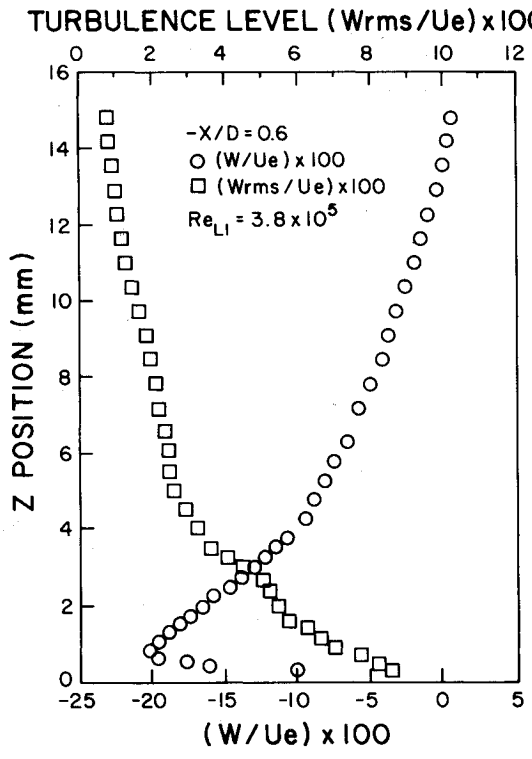

Fig. 14 Vertical velocity and turbulence level profiles for cylinder 3 at $-X/D=0.6$, $Y/D=0$, and $Re_{L_1}=3.8\times10^5$.

The postulated mean streamline pattern on the axis of symmetry, which is given by Fig. 4, requires the presence of positive streamwise velocities close to the surface slightly upstream of the secondary and tertiary separation lines. Figure 4 also indicates that the vertical velocities remain positive across the boundary layer in the vicinity of secondary and tertiary separation lines. Figure 4 also stipulates that during a streamwise traverse along various $Z=$ const lines, the vertical velocity changes sign more than once. The velocity measurements of this study, however, do not confirm such a flowfield pattern. It can be hypothesized that the locations of the vortex centers are time dependent, but the time-averaged surface locations where the vortices are shed remain approximately constant. Then the streamline pattern given in Fig. 4 can be considered as one of the possible streamlines which succeed each other in time. Tobak and Peake[13] give such a postulated sequence of the cyclic vortex structures in low-speed flow past a cylinder. The unsteady character of high-speed laminar flow can be similar to the cyclic nature of low-speed flow. However, further study is required to understand the unsteady aspects of the flowfield.

IV. Conclusions

An experimental investigation of supersonic flow past a cylindrical obstacle on a flat plate was made at Mach 2.36. In the laminar flow regime, oil flow visualization revealed three separation lines on the flat plate ahead of the cylinder. The maximum separation distance was approximately eight-cylinder diameters from the cylinder leading edge. The extent of separation was independent of the cylinder height-to-diameter ratio (H/D) for H/D values greater than approximately 4. The "free-interaction hypothesis" was observed to be valid on the axis of symmetry. Pressure rise through separation and pressure plateau levels were found to be similar to those of two-dimensional laminar flows. Large streamwise and spanwise pressure gradients were observed within an approximately two-cylinder-diameter vicinity of the cylinder axis. The maximum magnitudes of the negative streamwise and vertical velocities were approximately 20% of the freestream velocity. A postulated flowfield structure, which was suggested by oil flow visualization, could not be confirmed. The velocity measurements indicated an unsteady flow structure.

Acknowledgments

This study was supported by the NASA Ames Research Center under the Graduate Research Program in Aeronautics and Air Transportation, Grant NGR-05-003-451.

References

[1]Sedney, R. and Kitchens, C. W., "The Structure of Three-Dimensional Separated Flows in Obstacle, Boundary-Layer Interactions," AGARD CP-168, Paper 37, 1976, pp. 1-15.

[2]Korkegi, R. H., "Survey of Viscous Interactions Associated with High Mach Number Flight," *AIAA Journal*, Vol. 9, May 1971, pp. 771-784.

[3]Sedney, R., "A Survey of the Effects of Small Protuberances on Boundary-Layer Flows," *AIAA Journal*, Vol. 11, June 1973, pp. 782-792.

[4]Sedney, R. and Kitchens, C. W., "Separation Ahead of Protuberances in Supersonic Turbulent Boundary Layers," *AIAA Journal*, Vol. 15, April 1977, pp. 546-552.

[5]Dolling, D. S. and Bogdonoff, S. M., "Blunt Fin-Induced Shock Wave/Turbulent Boundary-Layer Interaction," *AIAA Journal*. Vol. 20, Dec. 1982, pp. 1674-1680.

[6]Dolling, D. S. and Bogdonoff, S. M., "An Experimental Investigation of the Unsteady Behavior of Blunt Fin-Induced Shock Wave Turbulent Boundary Layer Interaction," AIAA Paper 81-1287, June 1981.

[7]Avduevskii, V. S. and Medvedev, K. I., "Physical Properties of the Flow in the Separation Region for Three-Dimensional Interaction of a Boundary Layer with a Shock Wave," *Journal of Fluid Dynamics*, Vol. 2, No. 1, 1967, pp. 17-22.

[8]Young, F. L., Kaufmann, L. G., and Korkegi, R. H., "Experimental Investigation of Interaction Between Blunt Fin Shock Waves and Adjacent Boundary-Layers at Mach Numbers 3 and 5," Aerospace Research Laboratories, ARL 68-0214, Dec. 1968.

[9]Hung, F. T. and Clauss, J. M., "Three-Dimensional Protuberance Interference Heating in High Speed Flow," AIAA Paper 80-0289, Jan. 1980.

[10]Özcan, O., "An Experimental Investigation of Three-Dimensional Boundary-Layer Separation in Supersonic Flow Past a Circular Cylinder on a Flat Plate," Ph.D. Thesis, University of California, Berkeley, 1982.

[11]Hill, W. G., "Analysis of Experiments on Hypersonic Flow Separation Ahead of Flaps Using a Simple Flow Model," Grumann Research Memo. RM-393, 1967.

[12]Chapman, D. R., Kuehn, D. M., and Larson, H. K., "Investigation of Separated Flows in Supersonic and Subsonic Streams with Emphasis on the Effects of Transition," NACA 1356, 1958.

[13]Tobak, M. and Peake, D. J., "Topology of Two-Dimensional and Three-Dimensional Separated Flows," AIAA Paper 79-1480, July 1979.